Fractal Fourier spectra of Cherry flows

Michael A. Zaks

Department of Nonlinear Dynamics, Institute of Physics
Potsdam University, Postfach 601553, D-14415 Potsdam Germany
zaks@agnld.uni-potsdam.de

Abstract

Flows on the 2-torus with points of equilibrium are considered. Numerical observations suggest that, for the case of trajectories with irrational rotation numbers, power spectra are singular continuous. Dynamics is adequately represented by a symbolic sequence built from four symbols with the help of a substitution rule. This rule effectively takes into account the slowing down of the motion during passages near the saddle point and the superexponential scaling of returns onto a secant line.

Keywords: singular continuous spectrum; autocorrelation: rotation number.
PACS: 05.45.-a, 02.30.Hq

1 Introduction

Equations reducible to flows on 2-tori are encountered in different branches of science. In many cases, such dynamical systems possess no steady states: thus, in the textbook example of a 2-torus flow governing the dynamics of a periodically perturbed oscillator, the monotonic growth of the phase of the force forbids the existence of static equilibria. However, flows on 2-tori arise also in the autonomous setup where the evolution does not need to be monotonic. Examples of vector fields on low-dimensional tori which possess fixed points, appear in various physical contexts: charged particle transport in toroidal plasma fusion devices in the approximation of several electrostatic plane waves [1,2], charge-density wave transport[3], forced two-dimensional viscous flows [4], phase approximation to the dynamics of coupled solid state lasers interacting with an injected field [5], etc.

Since chaos in a continuous dynamical system is only possible if the dimension of its phase space exceeds two, dynamics on two-dimensional manifolds may appear simple. However, the question about the spectral properties of such flows is still not completely answered. Kolmogorov proved that the spectrum of a Hamiltonian flow on a 2-torus with an irrational rotation number is discrete, provided that two conditions are satisfied: the flow has no fixed points, and the rotation number cannot be anomalously well approximated by rationals [6];

his conjecture that violation of the latter condition could produce continuous spectrum, was later confirmed in [7]. Spectral properties are related to the ergodic property of mixing [8]; absence of mixing for a flow without fixed points on a 2-torus was demonstrated in [9]. In the present paper, we remove the remaining restriction and allow the vector field to possess fixed points. According to numerical results, in this case the Fourier spectrum of the trajectory with irrational rotation number is supported by a fractal set.

In Sect.2 an exemplary 2-parameter family of equations on a 2-torus is introduced. In Sect.3 the characteristics of the Fourier spectral measure are discussed. Numerically evaluated autocorrelation function indicates that the power spectrum of the flow with irrational rotation number is neither discrete nor absolutely continuous but fractal. A straightforward symbolic description based solely on topology of the orbit, fails to reproduce the unusual spectral properties of the flow. This discrepancy is due to the extreme variation of return times which is not contained in the Poincaré map. Sect.4 describes modification of the symbolic representation by incorporating metric information about dynamics. For this purpose, we utilize the fact that the return map is a discontinuous circle map for which the accumulation of closest returns to the critical point is described by the superexponential scaling law. The modified substitution rule produces a symbolic code whose spectral characteristics are in good correspondence with those of the original continuous flow. In the concluding part of the paper we argue that our particular example represents a typical case and, hence, the results apply to a wide class of flows with fixed points on the 2-torus.

2 A sample Cherry flow

In the generic case of a flow with fixed points on a 2-torus, at least one of these points should be a saddle. For the flows with rational rotation numbers, existence of saddle points permits the formation of homoclinic trajectories which can give birth to the respective closed orbits. The implications in the case of irrational rotation numbers are more far-reaching. The qualitative differences were described by Cherry [10] who constructed an analytical example of a vector field on a torus with a saddle, a source and non-trivial recurrent trajectories. By the term "Cherry flow" we will denote below a flow on a 2-torus which has fixed points and an irrational rotation number. We restrict ourselves to the simplest example when there are only two fixed points (Fig.1a), one of them a saddle and the other one a source: the latter may be either an unstable node or an unstable focus. Flows with one sink and one saddle turn into our case when viewed in reversed time. For the description of geometric properties of Cherry flows see e.g. [11,12]; typical bifurcation sequences were investigated in [13].

As an example, we consider the family

$$\begin{aligned} \dot{x} &= 1 + \sin y - \sin x \sin y \\ \dot{y} &= b + \cos x - K \cos x \cos y \end{aligned} \tag{1}$$

which is a generalization of equations arising in the context of forced spatially periodic steady

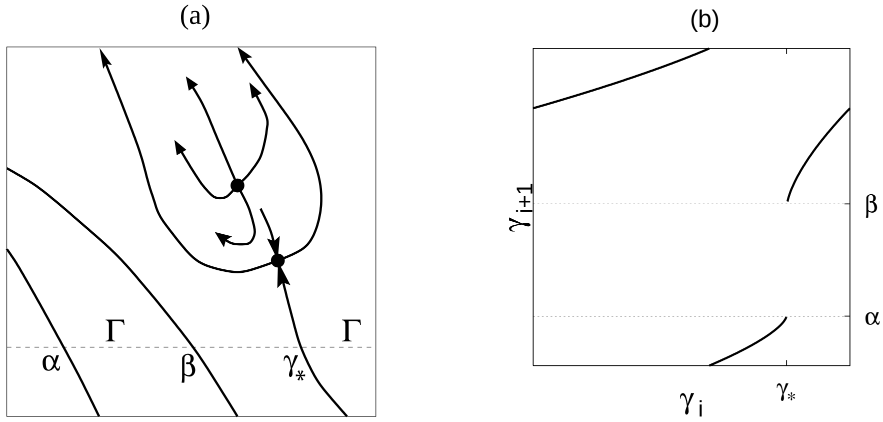

Fig. 1. (a) Geometry of the Cherry flow; Γ: global secant on the torus; α, β, γ_*: intersections of Γ with invariant manifolds of the saddle point.
(b) Return mapping on Γ (γ: coordinate along the secant).

motions of incompressible viscous fluid [4]. The algebraic expressions which, in terms of parameters b and K, ensure the existence of steady solutions of Eqs.(1), are too cumbersome to be quoted explicitly; below we deal with the ranges of values of b and K where such solutions are present.

To compute the rotation number on the torus T^2, we introduce a lift of the flow from T^2 to the plane R^2 [13]. For the case of a flow with a source, take the initial conditions (x_0, y_0) which do not belong to the stable manifold of a fixed point, and consider the forward limits of $x(t)$ and $y(t)$. The rotation number is defined as $\rho = \lim_{t\to+\infty} y(t)/x(t)$. If the flow has a sink instead of a source, the initial conditions should be chosen outside the unstable manifold of the saddle point, and the limit should be taken at $t \to -\infty$; for the conservative case, either of the limits will do.

We begin with this conservative flow. At $K = 1$ Eqs.(1) describe an area-preserving flow with the Hamiltonian $H(x, y) = -x + by - \cos y - \sin x + \sin x \cos y$. For $-1.56644 < b < 1.56644$, the vector field has two fixed points: a center and a saddle. The center is surrounded by closed curves which fill the "vortex" V encircled by the separatrix of the saddle point (Fig.2a). The rotation number for the points outside the vortex equals b; under irrational values of b each orbit which starts outside the vortex, is dense in $T^2 \setminus V$.

The situation for $K \neq 1$ is different. The degeneracy is removed, the continuum of closed curves disappears, and for $K > 1$ the center turns into the unstable focus (Fig.2b); for $K < 1$, the center becomes the stable sink (Fig.2c). In both cases the dense covering of the torus is replaced by the Cantor-like pattern.

The bifurcation diagram of Eqs.(1) on the plane of parameters b and K is briefly described in the Appendix. On this plane, Cherry flows exist on the continuum of curves; the curve which corresponds to a flow with rotation number ρ, passes through the point $(b = \rho, K = 1)$. We choose the curve corresponding to the inverse "golden mean" rotation number: $\rho = \sigma^{-1} = (\sqrt{5} - 1)/2$. A typical phase portrait of the attracting set is shown in Fig.2b; here, $K = 3/2$

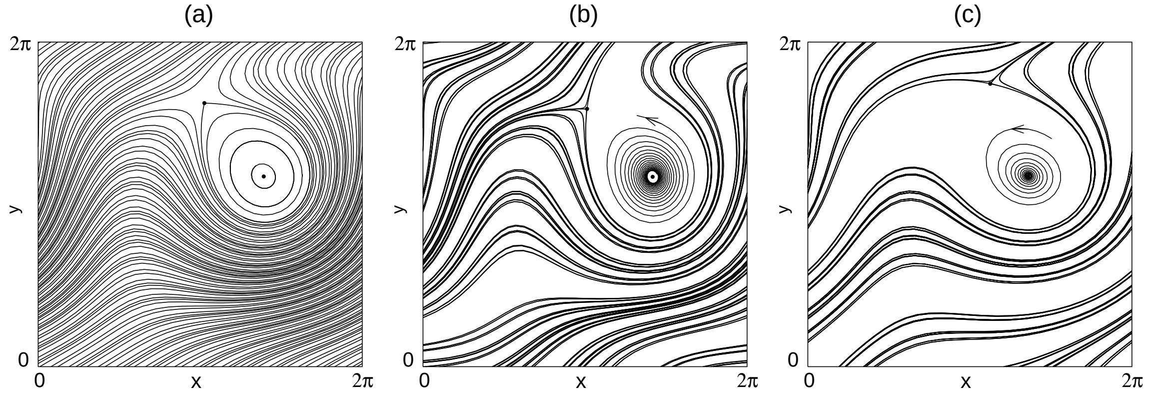

Fig. 2. Phase portraits of Eqs.(1) for flows with inverse golden mean rotation number.
(a) Hamiltonian flow: $K = 1, b = (\sqrt{5} - 1)/2$; (b) saddle and source: $K = 3/2, b = 0.58766578\ldots$; (c) saddle and sink: $K = 1/2, b = 0.60398604\ldots$.

and $b = 0.58766578\ldots$. In the course of winding around the torus, the orbit approaches the saddle point and departs from it; the distance between the orbit and the saddle is not bounded from below. During such passages the velocity of the imaging point can become arbitrarily small. This property has been shown to lead to the presence of the fractal component in the power spectrum [14].

3 Autocorrelations and Fourier spectra on orbits with irrational rotation numbers

Since we expect that the support of Fourier spectra can be concentrated on fractals, direct numerical computation of such spectra may prove to be a fragile procedure. For this reason, instead of insecure estimates in the frequency domain, we will mainly work in the time domain and use the more robust tool: autocorrelation function. Autocorrelation function $C(\tau)$ for the time-dependent observable $\xi(t)$ is introduced as

$$C(\tau) = \frac{\langle \xi(t)\xi(\tau + t)\rangle - \langle \xi(t)\rangle^2}{\langle \xi(t)^2\rangle - \langle \xi(t)\rangle^2}$$

where the angular brackets denote averaging with respect to the time t. If ξ is a periodic function of t, $C(\tau)$ is also periodic, with maximal values equal to 1. For quasiperiodic motions, the values of τ which correspond to the peaks of $C(\tau)$, form a progression in which the ratios of consecutive terms yield the best rational approximations to the irrational rotation number; the magnitude of these peaks tends to 1. For the chaotic and stochastic processes, the increase of τ is accompanied by the asymptotic decay of $C(\tau)$.

Autocorrelation is the Fourier image of the spectral measure $\mu(\omega)$: $C(\tau) = \int d\mu(\omega)\, \exp(\mathrm{i}\omega\tau)$. There always exists a uniquely determined decomposition of the spectral measure into the pure-point component (discrete power spectrum) and the continuous one [15]. The latter, in its turn, is further decomposable into a part which is absolutely continuous with respect to

Lebesgue measure (absolutely continuous power spectrum) and a singular continuous part supported by a fractal set. This singular continuous spectral component will be a main object of our interest.

Along with $C(\tau)$ we will also employ the "integrated autocorrelation"

$$C_{\rm int}(T) = \frac{1}{T}\int\limits_0^T |C(\tau)|^2 d\tau\,.$$

Behavior of these two functions at asymptotically large argument values characterizes the spectral measure:

a) a necessary condition for a spectral measure to be purely absolutely continuous is the decay of autocorrelation: $\lim_{\tau\to\infty} C(\tau) = 0$ [8];
b) contribution of the pure point component into the power spectrum is proportional to $\lim_{T\to\infty} C_{\rm int}(T)$ [16].

Hence, if for sufficiently long time intervals the integrated autocorrelation decays to (nearly) zero, one can conjecture that the power spectrum includes no discrete component. If, further, the autocorrelation function itself does not display the tendency to a complete decay, the absolutely continuous component of the spectral measure also appears to be absent. Consequently, the process has a singular continuous Fourier spectrum. Further, the knowledge of the power law which characterizes the decay rate of $C_{\rm int}(T)$, allows one to evaluate the fractal properties of the set which supports the spectral measure: for T large, $C_{\rm int}(T) \sim T^{-D_2}$ where D_2 is the correlation dimension of this fractal set [17,18] (for the connections between the products of autocorrelations and the values of the other generalized fractal dimensions D_q, see [19]).

For computational purpose, it is convenient to "unfold" a torus onto a plane and consider an observable which is a continuous periodic function of coordinates x and y; immediate candidates are trigonometric functions like $\cos x$.

Typical autocorrelation functions for the flows whose rotation number equals the inverse golden mean, are presented in Fig.3; note the logarithmic timescale. Within the plotted time intervals the orbit performs $\sim$3000 turns around the torus. The parameter values in Fig.3a and Fig.3b correspond to the phase portrait shown in Fig.2b; the flow at $K = 2, b = 0.513061539446796\ldots$ used for the plots in Fig.3c and Fig.3d, is qualitatively similar to Fig.2b. Finally, the plots of autocorrelations in Fig.3e and Fig.3f correspond to the quasi-minimal set of the vector field from Fig.2c which has a saddle and a sink (recall that under $K < 1$ one of the fixed points is a stable focus).

As recognizable in the plots, the autocorrelation $C(\tau)$ does not return to the value of 1; this underscores the difference from the case of quasiperiodic dynamics. On the other side, repetitive minor peaks of $C(\tau)$ imply that the power spectrum cannot be absolutely continuous. On the logarithmic axis, the highest peaks form a nearly regular lattice; they are separated by the distance $\approx \sigma = (\sqrt{5}+1)/2$. As visualized by the plots of the integrated

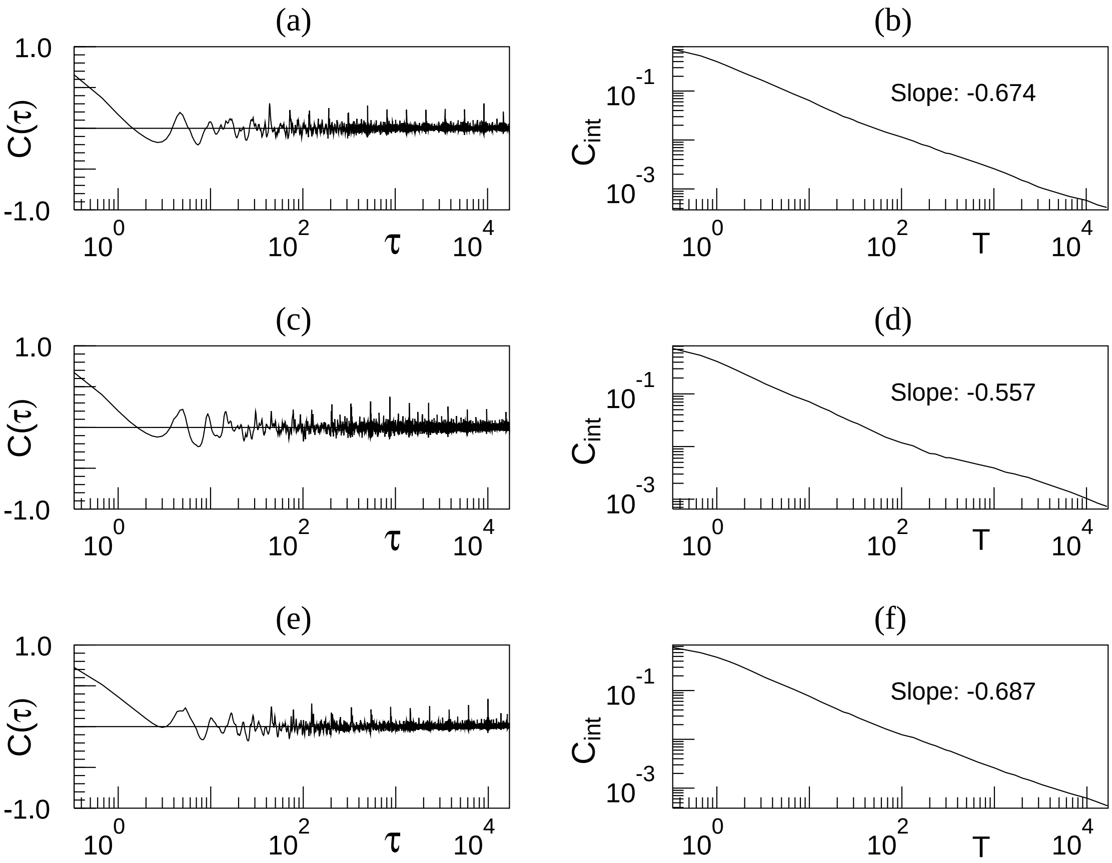

Fig. 3. Autocorrelation of observable $\cos x$ in flows with golden mean rotation number:
(a),(b): $K = 3/2; b = 0.58766578\ldots$ (vector field from Fig.2b);
(c),(d): $K = 2; b = 0.51306153\ldots$;
(e),(f): $K = 1/2; b = 0.60398604\ldots$ (vector field from Fig.2c).

autocorrelation which is apparently decaying, the spectrum also cannot include the discrete component. We can conjecture that the power spectrum is singular continuous; the dimension of the fractal set which supports the spectral measure, can be estimated from the slope of the $C_{\text{int}}(T)$ on log-log plots.

4 Symbolic coding

In this section, dynamics of the continuous flow is reduced to a much simpler discrete object: the sequence built over the finite set of symbols. Our aim is to obtain a symbolic string which adequately reproduces the spectral and correlation properties of the flow.

The most straightforward way to introduce the symbolic coding of the orbit involves the Poincaré map induced by the flow. Due to the presence of fixed points on the surface of the torus, such maps differ qualitatively from conventional circle mappings. Let us briefly describe their basic properties.

Let Γ be a global secant on the torus (Fig.1a). Since two separatrices of the saddle point return onto Γ in two different places (denoted, respectively, by α and β), the 1-dimensional map ϕ induced on Γ is not homeomorphic: not all of the points of Γ have preimages. This is a discontinuous circle map with a gap (Fig.1b). Since during the passage near the saddle the linear terms of the equations dominate, close to the discontinuity the mapping is described by the power law: for small positive ε, $\phi(\gamma_* + \varepsilon) - \beta \sim \varepsilon^\nu$, and $\alpha - \phi(\gamma_* - \varepsilon) \sim \varepsilon^\nu$. Here the saddle index $\nu = -\lambda_s/\lambda_u$ is the ratio of the negative eigenvalue λ_s and the positive eigenvalue λ_u of the Jacobian of the vector field taken at the saddle point. The properties of families of circle mappings with gaps were previously considered in the context of sequences of homoclinic ("gluing") bifurcations for flows in R^n, $n \geq 3$ [20–23]. The peculiarity of these mappings is the superexponential scaling near the irrational rotation numbers, both in the parameter space and along the state variable; the reason for this unusual scaling lies not in the power-law character of the map (the piecewise-linear map demonstrates it as well), but in the presence of the discontinuity. The flow with a sink is described by the same mapping in the reversed time. In this case the mapping is not everywhere defined on Γ: the backward orbits which start between the points α and β in Fig.1a end up in the sink and never return onto Γ. On extending the map to the whole of Γ by prescribing a constant value on $[\alpha, \beta]$, one arrives at the circle mapping with a flat interval. Such mappings have also been an object of extensive studies [24–27]. Thus, it has been proven that, under $\nu > 1$, the Hausdorff dimension of the non-wandering set of the map is strictly less than one [26]. For the opposite case of expanding maps with flat intervals, the Cherry flows have been shown to be, in a certain sense, "rare": parameter values corresponding to irrational rotation numbers have in the parameter space not only zero Lebesgue measure but also zero Hausdorff dimension [24]; under certain additional technical assumptions, each recurrent set of Γ with irrational rotation number has Hausdorff dimension zero [25].

The Poincaré map has one discontinuity and consists of monotonic branches; this suggests that the alphabet consisting of two symbols is sufficient for the adequate description of dynamics: the symbols mark the passages e.g. "below" and "above" the saddle point. The symbolic code for the inverse golden mean rotation number is the Fibonacci symbolic sequence $ABAABABA\ldots$ which can be obtained from the initial symbol A by means of repetitive substitutions (inflations) $\{A \to AB,\ B \to A\}$. On assigning to A and B numerical values, a symbolic code is turned into a sequence of numbers which can be further treated as time series. In this way the metric characteristics of the sequence (autocorrelation, Fourier spectrum, entropies, etc.) can be evaluated. The straightforward computation shows that the autocorrelation function $C(\tau)$ displays repetitive returns arbitrarily close to 1 (Fig.4a); hence, the power spectrum of the Fibonacci sequence is discrete. We see that the Fibonacci code, albeit correctly reproducing the pattern which the orbit follows during its winding around the torus, fails to reproduce the spectral properties of the Cherry flow. This does not mean that the chosen symbolic coding is not appropriate for the Poincaré map; the reason is deeper: the map itself also appears to have a discrete power spectrum (Fig.4b). Hence, the Poincaré map does not share the spectral properties of the underlying flow.

The situation in which the flows and their Poincaré maps have qualitatively different Fourier spectra, was discussed in [14]; the reason was found to lie in the unboundedness of the

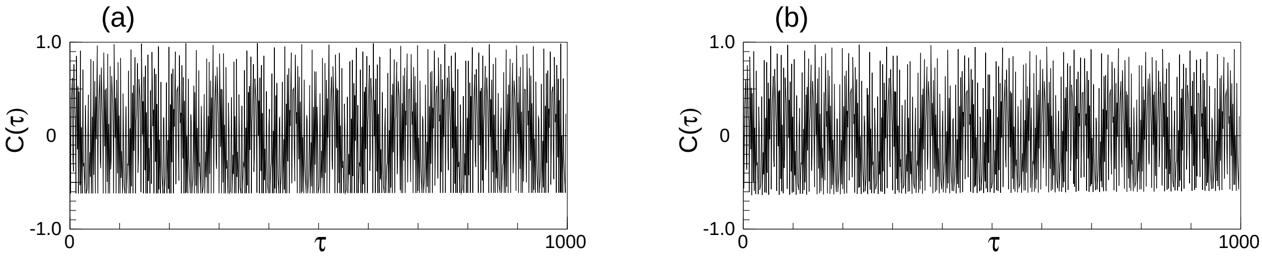

Fig. 4. Autocorrelation function for: (a) Fibonacci symbolic code;
(b): Poincaré mapping induced by the flow from Fig.2b.

return times onto the Poincaré surface in the phase space, resulting from presence of saddle points in the attractors of corresponding flows. In the case of Cherry flows the same mechanism is in action: trajectories can approach the saddle point arbitrarily close, and the time intervals between the returns onto a secant Γ can be arbitrarily long. The cause of the discrepancy is obvious: in the straightforward symbolic representation all turns of the trajectory around the torus are treated equally: each one, irrespectively of its temporal duration, is represented by a single symbol. The duration is characterized through strong variations: the turns during which the orbit passes close to the saddle point, require rather long time intervals. Consequently, the contribution of the protracted turns into the computation of averaged characteristics of the orbit, like the power spectrum, autocorrelation function etc., is significantly larger than that of the faster turns; this circumstance remains ignored by the Poincaré map.

To obtain an adequate symbolic description which recovers the metric characteristics of the process, one has to take into account the slowdown of the flow in the neighborhood of the saddle point. Certain symbols in the Fibonacci code must be doubled, tripled etc, depending on the length of the corresponding time intervals. Consider the Poincaré secant Γ parameterized by coordinate γ; let γ_*, as above, denote the coordinate of the intersection of Γ with the local stable manifold of the saddle point (Fig.1a). The length $\tau_{\rm r}$ of the time interval until the next return of an orbit onto Γ is a function of γ; it is easy to estimate that this function has a logarithmic singularity in the point γ_*:

$$\tau_{\rm r}(\gamma) \sim -\log|\gamma - \gamma_*| \tag{2}$$

The multiplicity (the number of repeats) of each symbol in the code should be proportional to the corresponding $\tau_{\rm r}$. In order to characterize the weight with which the individual symbols in the code contribute into the averaged characteristics, let us follow the approach of [28] and introduce the "residence time" R for the symbols. For the j-th symbol this time $R(j)$ is given by the length of time interval between the j-th and the $j+1$-th crossings of the Poincaré secant by the orbit starting at γ_*. (Strictly speaking, the orbit starting exactly at γ_* belongs to the local stable manifold of the saddle and never returns onto Γ; here and below under images of γ_* we mean, for shortness, either of the one-sided limits for $\gamma \to \gamma_*$; these limits correspond to two components of the unstable manifold of the saddle).

To estimate the distribution of residence times, scaling properties of the orbit should be taken into account. In the example of [28] the logarithmic singularity of return times was combined with the geometric (exponential) scaling on the attractor. In Cherry flows the situation is qualitatively different, and the construction of [28] cannot be directly applied. As already mentioned, in contrast to vector fields on tori without fixed points where under irrational rotation numbers the trajectories are dense, the trace of a Cherry flow on the secant Γ is a Cantor set (cf. Fig.2b). Keeping the inverse golden mean rotation number, consider the "Fibonacci returns" for the Poincaré mapping ϕ: the F_n-th images of γ_* where F_n is the n-th number in the Fibonacci series $\{1, 2, 3, 5, 8, 13\ldots\}$ [29]. The "odd" (corresponding to the odd n) and the even Fibonacci returns accumulate to γ_* from two opposite sides; as known from the analysis of gap maps [21–23], this accumulation is characterized through the superexponential scaling:

$$|\phi^{F_{n+2}}(\gamma_*) - \gamma_*| \sim |\phi^{F_n}(\gamma_*) - \gamma_*|^{\kappa} \tag{3}$$

where the rate of accumulation κ, in its turn, depends on the saddle index ν. The analysis of the corresponding renormalization operator shows that the relevant fixed point is singular: the renormalizing transformation cannot be properly linearized in its vicinity. For the values of ν close to 1 the respective κ can be estimated [22,23] as

$$\kappa(\nu) \approx \nu + \frac{\nu^2 + \sqrt{\nu^4 + 4\nu^3}}{2} \tag{4}$$

When n is large enough, the most part of $\tau_{\rm r}$ for the F_n-th return is spent in a very slow motion near the saddle point, and the contribution of relatively fast "global" passage around the torus is negligible. Combining (2) with (3), we obtain the residence times for the symbols with numbers F_n:

$$R(F_n) = \tau_{\rm r}\left(\phi^{F_n}(\gamma_*)\right) \sim G_{\rm o,e}\kappa^{n/2} \tag{5}$$

where the constants $G_{\rm o,e} > 1$ refer to odd and even n, respectively. According to Eq.(5), residence times for the Fibonacci returns form two geometric progressions with the same base κ.

The Cantor set on Γ has a hierarchical structure: it is composed of "clusters"; each cluster is organized around one of the Fibonacci returns; inside each cluster one observes the next level of self-similar hierarchy, and so on. As n grows, the size of the n-th cluster rapidly (obeying the double-exponential law) decreases. Since the gaps which separate the clusters are large compared to the cluster sizes, we can neglect the variation of return time inside each cluster. Therefore, as the representative timescale for each cluster we choose the value of $\tau_{\rm r}$ for the Fibonacci return from this cluster, as given by Eq.(5). Then, to compute the residence time for the j-th symbol in the code, one needs only to determine the number $N(j)$ of the cluster to which belongs the j-th image of γ_*. This $N(j)$ can be determined with the help of so-called Zeckendorf expansion [30] through which each natural number is in the unique way represented as a sum of non-neighboring Fibonacci numbers (e.g. 16=13+3, 133=89+34+8+2, etc.). The value of $N(j)$ is given by the place which the last (the smallest) term in the Zeckendorf expansion of j occupies in the Fibonacci series $\{1, 2, 3, 5, 8, 13\ldots\}$.

For the above examples, $N(16) = 3$ (the smallest term in the expansion is 3, which is the 3-rd Fibonacci number), $N(133) = 2$; obviously, $N(F_n) = n$. In this way, the residence time for j-th symbol becomes

$$R(j) = R\,(N(j)) = G\kappa^{N(j)/2} \tag{6}$$

where $G = G_\mathrm{o}$ ($G = G_\mathrm{e}$) if $N(j)$ is odd (even).

Since the residence time $R(j)$ effectively accounts for the contribution of the j-th turn of the orbit into the averaged characteristics, one can attempt to recover these characteristics numerically by computing them for the step function which admits only two values 1 and 0. In the plot of this function the j-th plateau has the height 1 if the j-th symbol of the Fibonacci code is A, and the height 0 if the respective symbol is B; the length of the j-th plateau is $N(j)$. Applied to the Fibonacci code, this procedure allows to recover fractal power spectra. On the symbolic level this means that the j-th letter in the symbolic Fibonacci code should be replaced by a string of $R(j)$ identical letters. In general, this does not work out, since the rate κ is non-integer, and we obtain the non-integer multiplicity for $R(j)$. A convenient integer example is delivered e.g. by $\kappa = 2$; according to Eq.(4) this requires the value of the saddle index $\nu \approx 2\sqrt{2} - 1 = 0.8284\ldots$ which in the Eqs.(1) corresponds to $K \approx 1.21$. We can choose a time unit to be G_o and include $\kappa^{1/2}$ into the rescaled G_e, then $R(F_{2n+1}) = \kappa^n$ and $R(F_{2n}) = G_\mathrm{e}\kappa^n$. Under $G_\mathrm{e} = 2$, this produces from the Fibonacci code $ABAABABA\ldots$ the string

$$A^{(1)}B^{(2)}A^{(2)}A^{(1)}B^{(4)}A^{(1)}B^{(2)}A^{(4)}\ldots \tag{7}$$

where the bracketed indices denote the residence times, in other words the multiplicities with which the respective letters should be repeated.

The very same symbolic string (7) can be produced in a different way, with the help of the substitution rule applicable to the case of integer κ. The rule combines two parts: a part, responsible for the correct ordering of the orbit, and a part which reflects the growth of residence times due to hovering near the saddle after Fibonacci returns. Since the topology of the orbit is the same as for the flow without fixed points, the first part must be the Fibonacci substitution $\{A \to AB,\ B \to A\}$. The action of the second part should elongate the sequence for A; let us use the symbol D for the added “hovering” segment: $A \to ABD$. The substitution rule for D is $D \to C$, where C denotes the “hovering part” of the previous Fibonacci return. In its turn, after the substitution C is replaced by two (three in case of κ=3, etc.) symbols D: $C \to DD$. Assembling the parts together, we obtain an inflation rule acting on an alphabet of four letters:

$$A \to ABD, \quad B \to A, \quad C \to DD, \quad D \to C \tag{8}$$

It should be kept in mind that both A and C refer to the same branch of the Poincaré map; the other branch is represented by B and D. For this reason, while computing the quantitative characteristics of the symbolic sequence, the numerical values should be assigned to the letters pairwise: e.g. $A = C = 1,\ B = D = 0$.

The autocorrelation function and integrated autocorrelation for the symbolic code built with the help of the rule (8) are presented in Fig.5a,b respectively. Modification of the rule allows to reproduce the qualitative properties of the autocorrelation function computed directly from the orbit of the Cherry flow (cf. Fig.3a,c,e): the observed structure has moderate, log-periodic in τ peaks, typical for systems with singular continuous spectra. The quantitative correspondence, as measured by the logarithmic period which is close to the golden mean $\sigma = (\sqrt{5}+1)/2$, and by the decay rate of the integrated autocorrelation, is also quite satisfactory.

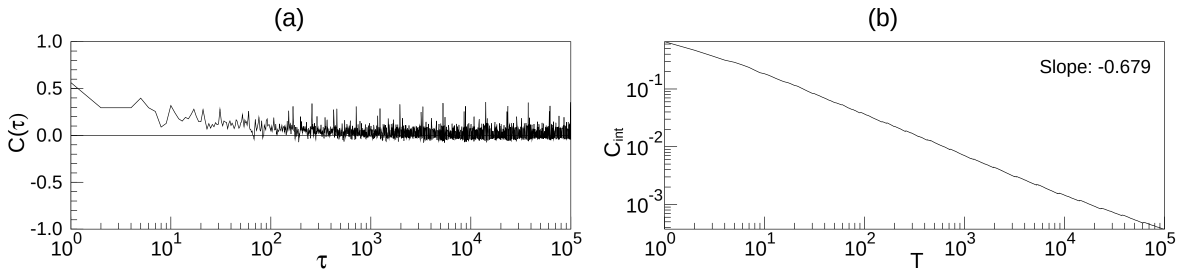

Fig. 5. Characteristics of symbolic code produced by substitution rule (8).
Code length: 4×10^6; (a) correlation function; (b) integrated autocorrelation.

5 Discussion

In order to obtain the symbolic sequence with correct spectral characteristics, topological properties of the trajectory (ordering of the turns, as reflected by the Fibonacci code) have to be combined with its metric properties (supexponential scaling of the nearest returns) and its dynamical characteristics (logarithmic divergence of return times). The crucial role is played here by the neighborhood of the saddle point. Each generic observable on the trajectory remains nearly constant during long periods of hovering near the saddle; durations and ordering of these hoverings are governed by the properties of the trajectory, and not of the observable itself. This argument shows that the singular continuous component should be present in the Fourier spectral measure of a generic observable.

Although the above results concentrate on the particular rotation number, they seem to be in some sense typical. Logarithmic periodicity for the lattice of peaks of the autocorrelation function follows from the periodicity of the expansion of the rotation number into the continued fraction: $\sigma^{-1} = \{1, 1, 1, \ldots\}$. The inverse golden mean σ^{-1} is slowly approximated by rationals; denominators of successive approximants F_n/F_{n+1} differ by a factor which tends to σ with $n \to \infty$. This growth factor determines the distance between the highest peaks of the autocorrelation function on the logarithmic timescale. For other “noble” irrationals (numbers with periodic expansions into continued fractions) log-periodicity of the peak lattice should persist; however, the convergence of approximants is faster, hence the peaks are more seldom. This is illustrated by Fig.6a where the autocorrelation function is plotted for the Cherry flow with the "silver mean" rotation number $\sqrt{2}-1 = \{2, 2, 2, \ldots\}$. For a "generic" rotation number, there is no periodicity among the coefficients of the continuous fraction expansion; hence the peak pattern is irregular. This can be seen in Fig.6b, where $C(\tau)$ is computed for the "randomly chosen" rotation number $0.441756079565\ldots = \{2, 3, 1, 3, 1, 4, 2, 1, 1, 3, 1, 1, 2, \ldots\}$.

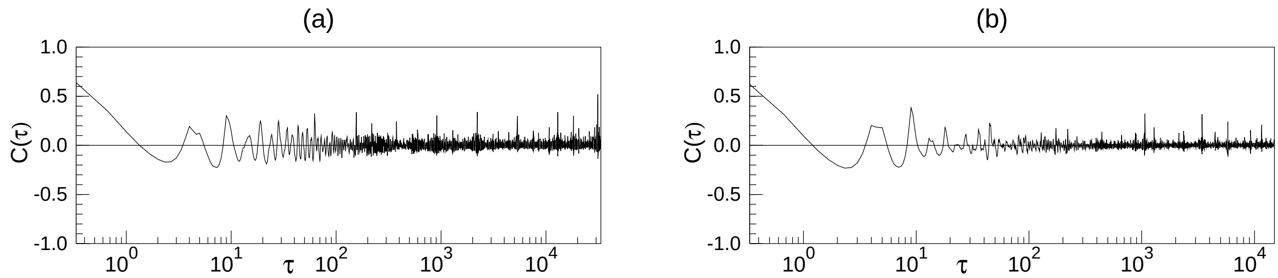

Fig. 6. Autocorrelation function for Cherry flows at $K = 3/2$:
(a) "silver mean" rotation number; $b = 0.38717552\ldots$
(b) rotation number 0.441756079565; $b = 0.40698228\ldots$

The substitution rule on the alphabet of four symbols can be easily generalized for other rotation numbers; the procedure should combine the symbolic 2-letter renormalization known from the usual circle map [31,21] and the elongation of residence times, described in the previous section. Thus, for a rotation number with expansion into the continuous fraction $\{n_1, \ldots, n_j, \ldots\}$ substitution on the j-th step should be

$$A \to B^{(n_j-1)}ABD, \quad B \to B^{(n_j-1)}A, \quad C \to DD, \quad D \to C \tag{9}$$

For rotation numbers with periodic or eventually periodic continued-fraction expansions, a finite set of substitutions would alternate in the regular manner, eventually resulting in the ordered lattice of peaks for the autocorrelation function. Non-periodic sequences of continuous fraction entries $\{n_i\}$ would produce disordered symbolic strings and, consequently, disordered peak pattern.

Irrespective of the periodicity of the continued fraction expansion, the presence of singular continuous component appears to be the common property both of Cherry flows and of substitution sequences which mimic this unusual kind of two-dimensional dynamics.

Another aspect which deserves to be mentioned here, is the role of power spectra as a criterion to separate chaotic processes from non-chaotic ones. Among the first tools exploited by experimentalists in their search for chaos in the experimental data was the Fourier analysis of time records [32,33], with continuous spectra being interpreted as the hallmark of chaotic dynamics, and discrete spectra indicating to non-chaotic behavior. Since that early work, this criterion has been often employed for the identification of the type of dynamics from experimental and numerical data. The above results suggest that certain precautions should be met: in case of processes with fractal power spectra, finite-length spectral sums may produce the false impression of the absolutely continuous spectrum and, hence, chaotic dynamics. This can be seen in Fig. 7 which shows the approximation to the power spectrum of the Cherry flow from Fig.2b, estimated from 2^{14} datapoints. Behavior of spectral sums under the increase of the dataset length should be checked: in case of the absolutely continuous spectrum, finite-length approximations converge to a bounded spectral curve, whereas the absence of such convergence indicates to the presence of singularities in the spectral measure.

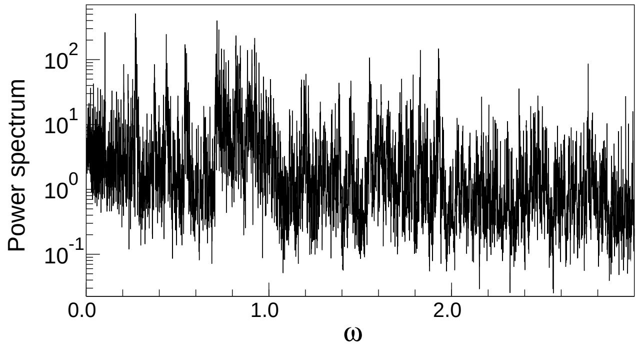

Fig. 7. Estimation of the power spectrum for the flow from Fig.2b. Length of the sample: 2^{14} points.

Acknowledgements

I am grateful to A. Pikovsky and J. Kurths for stimulating discussions. The valuable suggestions of the Referee on improving the quality of the manuscript are gratefully acknowledged.

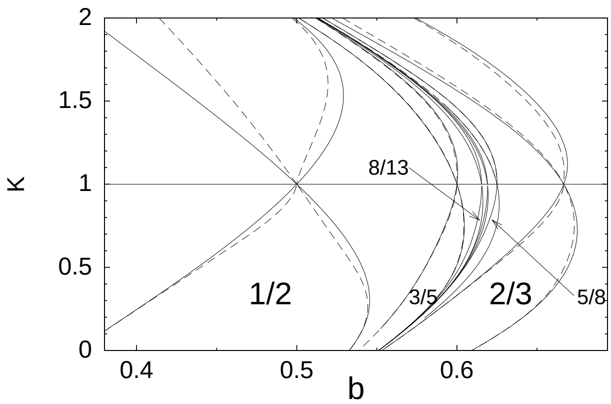

Fig. 8. Bifurcation diagram of Eqs (1). Labels denote rotation numbers;
solid lines: saddle-node bifurcations of periodic solutions;
dashed lines: homoclinic bifurcations of the saddle-point.

Appendix: Bifurcation sequences in the family (1).

The organizing element for the diagram of states on the parameter plane of the equations (1) is the line $K = 1$ on which the dynamics is Hamiltonian, and on which each rotation number ρ is represented by the point $b = \rho$. For rational values of ρ, the existence domains for periodic solutions with the corresponding rotation numbers open from these points into both directions ($K > 1$ and $K < 1$, respectively); for irrational ρ these points belong to the existence curves for the Cherry flows. In Fig.8 these domains are presented for the rotation numbers equal to the first 6 ratios of the consecutive Fibonacci numbers F_n/F_{n+1}.

The structure of the parameter plane is reminiscent of two-parameter families with quasiperiodic and periodic dynamics. Similarly to the Arnold tongues in such families, the domains of periodic behavior have wedge-like shape and are bounded by the lines of saddle-node bifurcations. However, in contrast to the Arnold tongues, inside these domains there are additional bifurcation lines which pass through the tips of the wedges: lines of homoclinic bifurcations. These lines divide each "tongue" into the inner region and two narrow sideband strips. In the narrow strips, close to the curves of tangent bifurcations, two periodic orbits are present: one stable and one unstable; this illustrates the statement proven in [34] that approximations to expanding Cherry flows possess at most two periodic trajectories. In the inner region only one periodic orbit exists. For $K > 1$ this is the stable one, which remains the unique attractor for the flow in the whole parameter domain. For $K < 1$ the picture is reversed; now the unstable periodic orbit is present everywhere inside the tongue, whereas the existence of the stable one is restricted to the strips outside the curves of homoclinic bifurcations. Inside the inner tongue, the only attractor of the flow is the stable fixed point; in the strips two attracting states coexist.

References

[1] J. H. Misguich, R. Nakach, Guiding center chaotic motion in three electrostatic waves, Phys. Rev. A **44** 3869–3888.

[2] G. Petschel, T. Geisel, Unusual manifold structure and anomalous diffusion in a Hamiltonian model for chaotic guiding center motion, Phys. Rev. A **44** 7959–7967.

[3] S. H. Strogatz, C. M. Markus, R. M. Westervelt, R. E. Mirollo, Collective dynamics of coupled oscillators with random pinning, Physica D **36** 23–50 (1989).

[4] M. A. Zaks, A. S. Pikovsky, J. Kurths, Steady viscous flow with fractal power spectrum, Phys. Rev. Lett. **77**, 4338–4341 (1996).

[5] A. I. Khibnik, Y. Braiman, T. A. B. Kennedy, K. Wiesenfeld, Phase model analysis of two lasers with injected field, Physica D **111**, 295–310 (1998).

[6] A. N. Kolmogorov, On dynamical systems with an integral invariant on a torus, Dokl. Akad. Nauk SSSR Ser. Mat. **93**, 763–766 (1953) [in Russian].

[7] M. D. Shklover, On classical dynamical systems on the torus with continuous spectrum, Izv. Vyssh. Uchebn. Zaved. Mat. 10, 113–124 (1967) [in Russian].

[8] I. P. Cornfeld, S. V. Fomin, and Ya. G. Sinai, *Ergodic Theory* (Springer, New York, 1982).

[9] A. V. Kochergin, On the absence of mixing for special flows over rotations of the circle and for flows on the two-dimensional torus, Sov.Math.Dokl. **13**, 949–952 (1972).

[10] T. M. Cherry, Analytic quasi-periodic curves of discontinuous type on a torus, Proc. London Math. Soc. **44**, 175–215 (1938).

[11] J. Palis and W. de Melo, *Geometric theory of dynamical systems: An introduction*, (Springer, New York,1982)

[12] I. Nikolaev, E. Zhuzhoma, Flows on 2-dimensional manifolds, Lecture Notes in Mathematics, **1705** (Springer, Berlin, 1999).

[13] C. Baesens, J. Guckenheimer, S. Kim, R. S. MacKay, Three Coupled Oscillators: Mode-locking, Global Bifurcations and Toroidal Chaos, Physica D **49**, 387–475 (1991).

[14] A. S. Pikovsky, M. A. Zaks, U. Feudel, and J. Kurths, Singular continuous spectra in dissipative dynamical systems, Phys. Rev. E **52**, 285–296 (1995).

[15] M. Reed, B. Simon, *Methods of modern mathematical physics*, Academic Press, NY, 1972.

[16] N. Wiener, The spectrum of an array, J. Math. and Phys. **6**, 145–157 (1926).

[17] R. Ketzmerick, G. Petschel, and T. Geisel, Slow decay of temporal correlations in quantum systems with Cantor spectra, Phys. Rev. Lett. **69**, 695–698 (1992).

[18] M. Holschneider, Fractal wavelet dimensions and localization, Commun. Math. Phys. **160**, 457–473 (1994).

[19] M. A. Zaks, A. S. Pikovsky, and J. Kurths, On the generalized dimensions for the Fourier spectrum of the Thue-Morse sequence, J. Phys. A: Math.Gen. **32**, 1523–1530 (1999).

[20] J.-M. Gambaudo, I. Procaccia, S. Thomae, and C. Tresser, New universal scenarios for the onset of chaos in Lorenz-type flows, Phys.Rev.Lett **57**, 925–928 (1986).

[21] I. Procaccia, S. Thomae, and C. Tresser, First return maps as a unified renormalization scheme for dynamical systems, Phys.Rev.A **35**, 1884–2001 (1987).

[22] D. V. Lyubimov, A. S. Pikovsky, and M. A. Zaks, Universal scenarios of transition to chaos via homoclinic bifurcations, in *Mathematical Physics Review, vol.8*, edited by S.P.Novikov (Gordon and Breach, Chur, 1989), 221–292.

[23] M. A. Zaks, Scaling properties and renormalization invariants for the "homoclinic quasi-periodicity", Physica D **62**, 300–316 (1993).

[24] C. Boyd, On the structure of the family of Cherry fields on the torus, Ergod. Th. & Dynam. Sys. **5**, 27–46 (1985).

[25] J. J. P. Veerman, Irrational rotation numbers, Nonlinearity **2**, 419–428 (1989).

[26] J. Graczyk, L. B. Jonker, G. Świątek, F. M. Tangerman, J. J. P. Veerman, Differentiable circle maps with a flat interval, Commun. Math. Phys. **173**, 599–622 (1995).

[27] P. Glendinning, Bifurcations and rotation numbers for maps of the circle associated with flows on the torus and models of cardiac arrhythmias, Dynam. Stability Systems **10**, 367–386 (1995).

[28] M. A. Zaks, A. S. Pikovsky, and J. Kurths, Symbolic dynamics behind the singular continuous power spectra of continuous flows, Physica D **117**, 77–94 (1998).

[29] Naturally, the full Fibonacci series reads $\{1, 1, 2, 3, 5, 8, \ldots\}$; to simplify the notation, we start the enumeration from zero: $F_0 = 1, F_1 = 1, \ldots$, and do not use the zeroth term.

[30] E. Zeckendorf, "Répresentation des nombres naturels par une somme des nombres de Fibonacci ou de nombres de Lucas", Bull. Soc. Roy. Sci. Liège **41**, 179–182 (1972).

[31] D. Rand, S. Ostlund, J. Sethna, E. Siggia, Universal properties of the transition from quasi-periodicity to chaos in dissipative systems, Physica D **8**, 303–342 (1982).

[32] J. P. Gollub, H. L. Swinney, Onset of turbulence in a rotating fluid, Phys. Rev. Lett., **35**, 927–930 (1975).

[33] J. P. Gollub and S. V. Benson, Many routes to turbulent convection, J. Fluid Mech., **100**, 449–470 (1980).

[34] W. de Melo, On the cyclicity of recurrent flows on surfaces, Nonlinearity **10** 311-319 (1997).